



How to cite:

International Edition: doi.org/10.1002/anie.202214117

German Edition: doi.org/10.1002/ange.202214117

A Shuttle-Free Solid-State Cu–Li Battery Based on a Sandwich-Structured Electrolyte

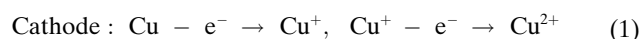
Huimin Wang⁺, Changhong Wang⁺, Matthew Zheng, Jianneng Liang, Ming Yang, Xingyu Feng, Xiangzhong Ren, Denis Y. W. Yu, Yongliang Li,^{*} and Xueliang Sun^{*}

Abstract: Cu–Li batteries leveraging the two-electron redox property of Cu can offer high energy density and low cost. However, Cu–Li batteries are plagued by limited solubility and a shuttle effect of Cu ions in traditional electrolytes, which leads to low energy density and poor cycling stability. In this work, we rationally design a solid-state sandwich electrolyte for solid-state Cu–Li batteries, in which a deep-eutectic-solvent gel with high Cu-ion solubility is devised as a Cu-ion reservoir while a ceramic $\text{Li}_{1.4}\text{Al}_{0.4}\text{Ti}_{1.6}(\text{PO}_4)_3$ interlayer is used to block Cu-ion crossover. Because of the high ionic conductivity (0.55 mS cm^{-1} at 25°C), wide electrochemical window ($>4.5 \text{ V vs. Li}^+/\text{Li}$), and high Cu ion solubility of solid-state sandwich electrolyte, a solid-state Cu–Li battery demonstrates a high energy density of $1485 \text{ Wh kg}_{\text{Cu}}^{-1}$ and long-term cyclability with 97% capacity retention over 120 cycles. The present study lays the groundwork for future research into low-cost solid-state Cu–Li batteries.

Introduction

There is an increasing demand for advanced battery technologies with high energy density, low cost, and unrivaled safety for applications in portable electronics, electrified vehicles, and renewable energy storage.^[1] Battery chemistries based on electrochemical dissolution/deposition of low-cost metal cathodes, e.g., Cu, Fe, and Ni, have attracted increasing interest because of their higher theoret-

ical capacities, abundance, environmental friendliness, and easy extraction.^[2] Rechargeable Cu cathode-based batteries, e.g., Cu–Li batteries, are particularly desirable since Cu metal readily undergoes a two-electron redox reaction even in a neutral electrolyte. Furthermore, adopting the low potential Li anode enables a high output voltage. In principle, the electrochemical reactions of a Cu–Li battery can be described as below:



During charging, metallic Cu is oxidized and dissolves in electrolytes, and Li^+ migrates to the anode and gets plated into Li metal. The stripping/plating of Cu occurs at the cathode, accompanied by the plating/stripping of Li at the anode. Cu cathode offers a high theoretical capacity of $838 \text{ mAh g}_{\text{Cu}}^{-1}$ based on its two-electron electrochemical reaction.^[3] Besides, Cu cathode can be scaled up easily owing to its mature industrial process in commercial lithium-ion batteries. However, research into rechargeable Cu–Li batteries throughout the last decade has failed to compete with research in other battery systems, which can be attributed to long-standing challenges from the electrolyte, namely 1) limited Cu species solubility; 2) shuttle effect of Cu species, and 3) limited ionic conductivity.

Over the past decade, some attempts have been made to address these challenges. For instance, Wang et al. used an aqueous electrolyte (2 M LiNO_3) to increase the solubility of Cu species and demonstrated a $\approx 3.2 \text{ V}$ Cu–Li battery.^[3a] Though the increased solubility, this electrolyte design could pose severe safety concerns due to the possible contact between highly reactive Li and water. To avoid such safety concerns and enhance the Li anode compatibility, carbonate-based electrolytes with a lower solubility of Cu species have been proposed to replace the aqueous electrolyte in Cu–Li batteries.^[3d,4] However, this design sacrifices the Cu-ion solvating ability. Accordingly, a significant amount of carbonate electrolytes can be added, which compromises the overall energy density of Cu–Li batteries.^[2c] To overcome the Cu-ion shuttle effect, we have proposed several effective strategies in 3 V Cu–Al batteries, including 1) the adoption of concentrated electrolyte in combination with an ion-selective membrane^[5] and 2) engineering interaction between Cu-solvation complex and polypropylene membranes.^[6] Although a decent battery cyclability can be realized in these cases, a large amount of

[*] Dr. H. Wang,⁺ Dr. J. Liang, M. Yang, X. Feng, Prof. Dr. X. Ren, Prof. Dr. Y. Li
 College of Chemistry and Environmental Engineering, Shenzhen University
 3688 Nanhai Blvd, Nanshan, Shenzhen, Guangdong 518060 (P. R. China)
 E-mail: liyli@szu.edu.cn

Dr. H. Wang,⁺ Dr. C. Wang,⁺ M. Zheng, Prof. Dr. X. Sun
 Department of Mechanical and Materials Engineering, University of Western Ontario
 1151 Richmond St, London, Ontario N6A 3K7 (Canada)
 E-mail: xsun9@uwo.ca

Dr. D. Y. W. Yu
 School of Energy and Environment, City University of Hong Kong
 83 Tat Chee Ave, Kowloon Tong, Hong Kong (P. R. China)

[†] These authors contributed equally to this work.

metallic cathode is required, resulting in a small practical energy density. Moreover, this desirable Cu-ion confinement is often at the expense of limited ionic conductivity of electrolytes, resulting in poor battery kinetics. Therefore, continuous efforts to design an appropriate electrolyte for Cu–Li batteries is highly desired. Based on our understanding, several criteria must be simultaneously met in the electrolyte design to attain a high-performance rechargeable Cu–Li battery, including: 1) high compatibility with respect to Li, 2) high solubility of Cu ions, 3) high ion selectivity to completely block the shuttle of Cu species and 4) sufficient ionic conductivity at room temperature.

For this purpose, we design a solid-state sandwich electrolyte with a structure of DES gel/LATP/DES-FEC gel for solid-state Cu–Li batteries for the first time (Figure 1). The key features of this Cu–Li battery are as follows: first, a deep-eutectic-solvent-based gel (DES gel) is developed to dissolve and retain electrochemically-generated Cu ions at the cathode side because of its unusually high solubility of metal species.^[7] Second, a DES gel layer with 10 wt % fluoroethylene carbonate additive (DES-FEC gel) is devised to stabilize the Li plating/stripping at the anode side. Third, a $\text{Li}_{1.4}\text{Al}_{0.4}\text{Ti}_{1.6}(\text{PO}_4)_3$ (LATP) interlayer is used to prevent the crossover of Cu ions and allow the exclusive transportation of Li^+ . The as-prepared solid-state sandwiched electrolyte (DES gel/LATP/DES-FEC gel) exhibits a sufficient Li^+ conductivity (0.55 mS cm^{-1} at 25°C) and wide electrochemical window (4.5 V vs Li^+/Li). A rechargeable solid-state Cu–Li battery based on this solid-state sandwich electrolyte delivers a high reversible capacity of $511 \text{ mAh g}_{\text{Cu}}^{-1}$, dramatically improved compared with previously reported values.^[2c,6] Furthermore, this battery exhibits a capacity retention of 97 % over 120 cycles, accompanied by a specific energy of $1451 \text{ Wh kg}_{\text{Cu}}^{-1}$ (at $200 \text{ mA g}_{\text{Cu}}^{-1}$). A capacity of $325 \text{ mAh g}_{\text{Cu}}^{-1}$ could still be achieved even when the Cu–Li battery was cycled at 1000 mA g^{-1} , paralleling a specific energy of $635 \text{ Wh kg}_{\text{Cu}}^{-1}$. It should be mentioned that this solid-state sandwich electrolyte design is also applicable to other metal-cathode batteries.

Results and Discussion

To break the trade-off between Cu species solubility and Li metal compatibility, herein, we employ deep eutectic solvents (DESs). DESs are eutectic mixtures of Lewis acids and bases that are often cheaply obtained and easily prepared.^[8] Because of its unusually high capability of dissolving metal species, DESs have been used to recycle the transition metal oxide cathodes of Li-ion batteries.^[7] Besides, DESs also show decent compatibility with the Li anode.^[9] Therefore, DES-based electrolytes show high promise to work as the Cu-ion reservoir at the cathode and stabilize Li plating/stripping reaction at the anode. The solid-state sandwich electrolyte (DES gel/LATP/DES-FEC gel) was constructed by stacking the DES gel, LATP pellet, and DES-FEC gel. To prepare the DES gel, a series of DESs were first obtained by mixing lithium bis(trifluoromethanesulfonyl)imide (LiTFSI) and succinonitrile (SCN) at different molar ratios (1:4, 1:7, 1:10, 1:13 and 1:16). It is interesting to note that though each individual component (LiTFSI and SCN) are solid state at room temperature, the mixed two solids turn into a liquid eutectic mixture when heating at 60°C and maintain liquid form even after cooling down to room temperature (Figure 2a). The Li^+ conductivities of DESs increase with increasing SCN content, which is ascribed to the reduced viscosity and increased free SCN molecules (Supplementary Figure 1). However, the eutectic mixture would be destroyed with the precipitation of crystals when continuing to increase the SCN content up to 16 (Supplementary Figure 2). Therefore, we keep the LiTFSI/SCN ratio at 1:13 in the following test to maintain a sufficient Li^+ conductivity (4.12 mS cm^{-1} at 20°C) and a liquid state within a wide temperature range.^[10]

10 wt % ethoxylated trimethylolpropane triacrylate (ETPTA) monomer and 1 wt % azobisisobutyronitrile (AIBN) initiator were further dissolved into the DES with a molar ratio of $\text{LiTFSI}/\text{SCN}=1:13$, which transforms the liquid into a translucent gel by ETPTA polymerization at 70°C (Figure 2b and top inset). A free-standing DES gel layer was obtained with a thin glass fiber disc as the substrate (low inset in Figure 2b and Supplementary Figure 3). Figure 2c shows the FTIR patterns of the ETPTA

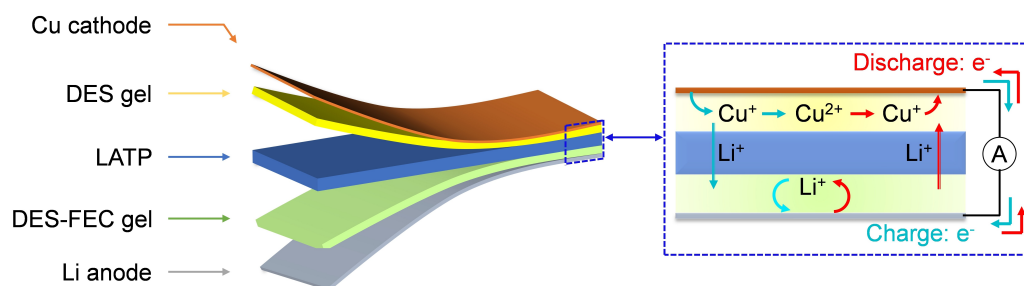


Figure 1. Schematic of a solid-state Cu–Li battery. A solid-state Cu–Li battery consists of a Cu cathode, a Li anode, and a sandwich electrolyte. The sandwich electrolyte was constructed by stacking the DES gel, LATP pellet, and DES-FEC gel together. During cycling, stripping/plating of Cu and Li occurs at the cathode and anode, respectively.

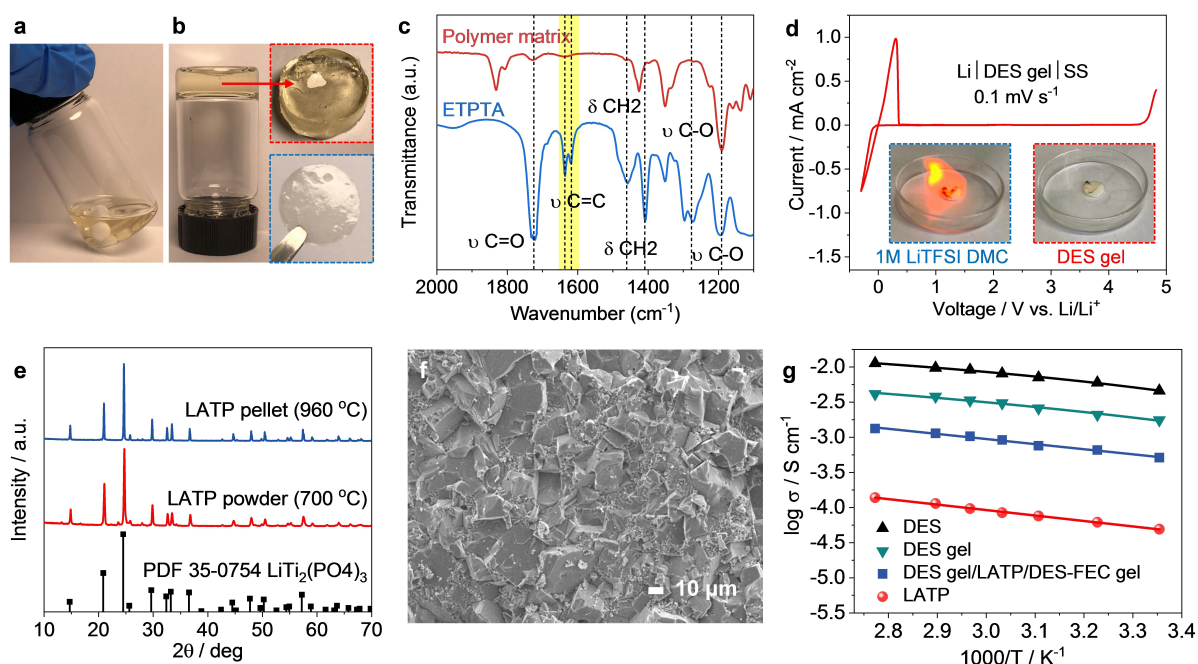


Figure 2. Characterizations of solid-state sandwich electrolytes. a, b) Optical images of a) liquid DES (m.r. LiTFSI/SCN = 1:13) and b) DES gel. Insets of (b): translucent DES gel (top) and free-standing gel layer supported with thin glass fiber (bottom). c) FTIR spectra of the ETPTA monomer and polymer matrix of gel. d) Electrochemical stability of DES gel at 0.1 mV s^{-1} ; insets: optical images of the 1 M LiTFSI DMC electrolyte (low left) and DES gel (low right) under a combustion test. e) XRD patterns and f) cross-sectional SEM images of LAMP pellets. g) Ionic conductivities of liquid DES, DES gel, LAMP, and DES gel/LAMP/DES-FEC gel as a function of temperature (m.r. LiTFSI/SCN = 1:13).

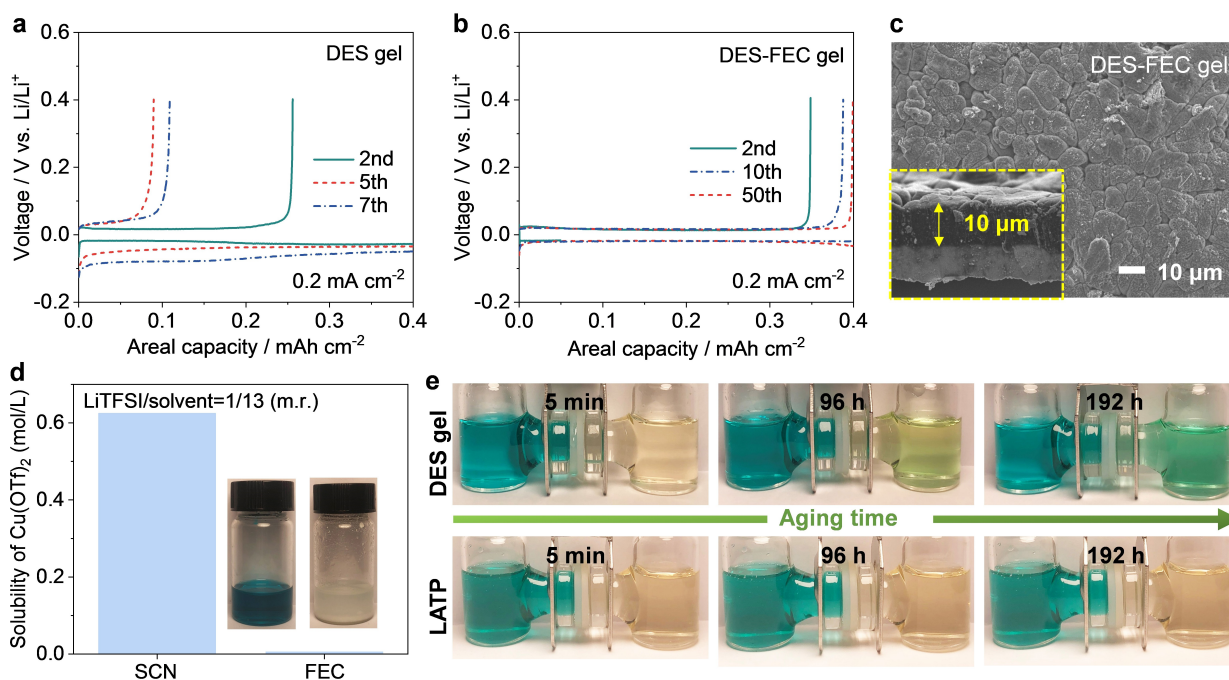


Figure 3. Function of each component in the solid-state sandwich electrolyte. Plating/stripping of Li on Ti current collector in a) a Li|DES gel|Ti foil cell and b) a Li|DES-FEC gel|Ti foil cell at 0.2 mA cm^{-2} with a capacity limitation of 0.4 mAh cm^{-2} . c) Top FE-SEM images of Li dense deposition on Ti current collector in a Li|DES-FEC gel|Ti foil cell. Inset: the corresponding cross-sectional image of Li layer on Ti foil. d) Comparison of Cu species solubility in DES and FEC-based electrolyte (m.r. LiTFSI/solvent = 1:13). Insets: the optical pictures of Cu species dissolved in DES (left) and FEC-based electrolyte (right). e) Visual observation of Cu ions crossover through a DES gel membrane (upper panel) and a LAMP pellet (lower panel) at room temperature in an H-type cell. Left and right tanks were filled with DES-7 mol% Cu(OTf)₂ and DES liquid electrolytes, respectively.

monomer and the as-prepared polymer matrix. The peak centered at 1620 cm^{-1} is attributed to the vibration of $\text{C}=\text{C}$ in ETPTA,^[11] which vanished after polymerization at 70°C . This phenomenon indicates the successful polymerization of ETPTA with the presence of an AIBN initiator when heating at 70°C . The DES-FEC gel layer was prepared by the same gelation procedures with an additional 10 wt % FEC in the DES. The Mechanical properties of the as-prepared DES and DES-FEC gel layers were evaluated via stress-strain curves in tensile tests (Supplementary Figure 4a), and Young's modulus can be calculated to be 435 MPa and 415 MPa, respectively, based on the elastic regions at the low strain. The SEM images of DES gel and DES-FEC gel layers can be found in Supplementary Figure 4b,c.

A gel with high oxidation stability is highly desirable to allow the adoption of high-voltage cathode materials. Herein a Li|DES gel|stainless-steel cell was made to examine the oxidation stability of DES gel at a scan rate of 0.1 mV s^{-1} . We can see that the as-prepared DES gel stabilizes up to 4.5 V vs. Li^+/Li . In addition, when scanning the cell to the lower voltage region, a pair of reversible redox peaks at $\approx 0\text{ V}$ is also observed, corresponding to the plating/stripping of Li. The DES gel's excellent oxidation stability and Li compatibility suggest its feasibility for developing $\approx 3\text{ V}$ Cu–Li batteries. In addition, a flame test shows that the as-prepared DES gel is non-flammable (right insert in Figure 2d). Negligible weight loss is found under 150°C in thermogravimetric analysis (Supplementary Figure 5b). In contrast, conventional 1 M LiTFSI in dimethyl carbonate (DMC) electrolyte is highly flammable (left inset

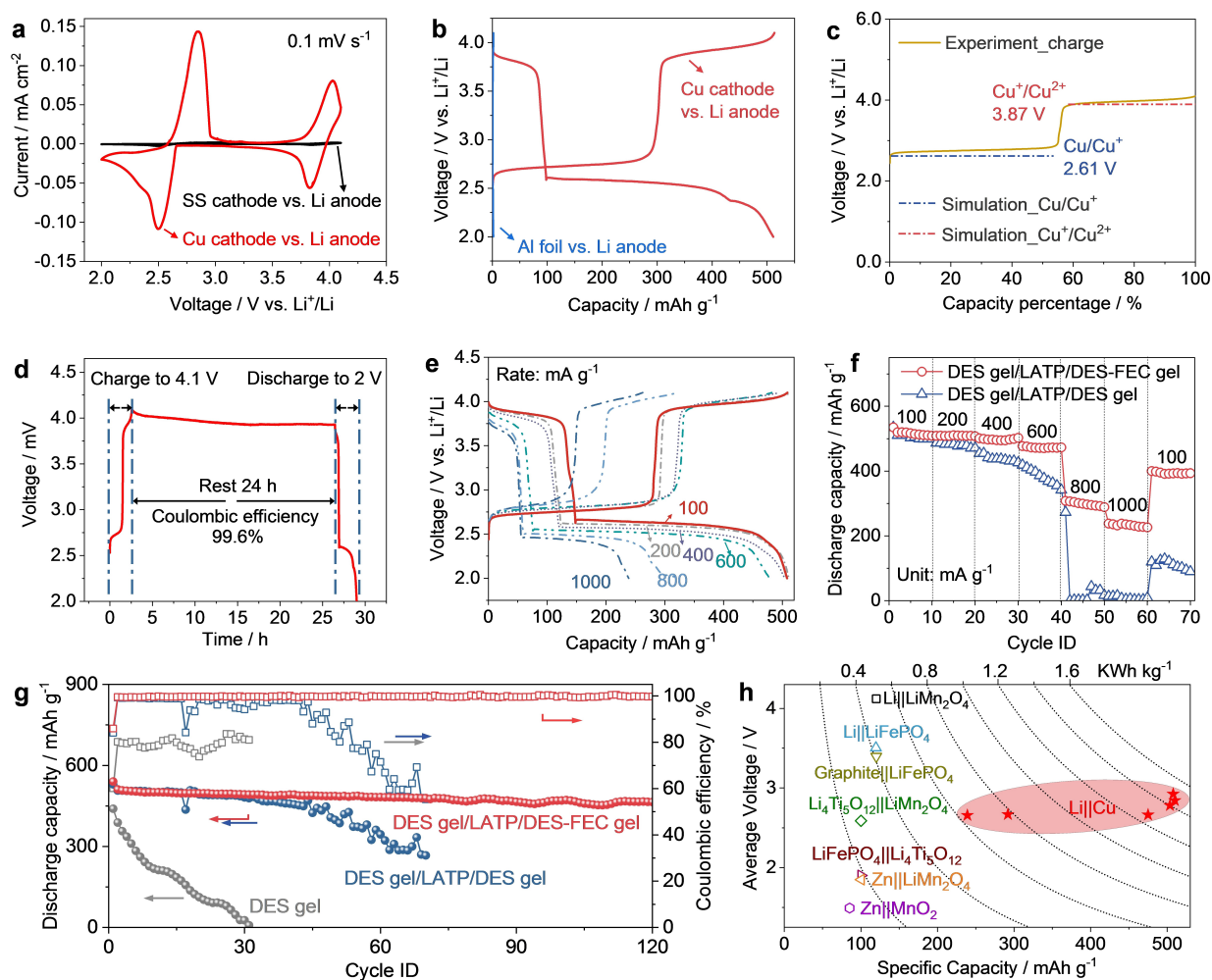


Figure 4. Cu cathode reaction mechanism and electrochemical performance of solid-state Cu–Li batteries. a) Cyclic voltammogram of a Cu–Li battery separated with DES gel/LATP/DES-FEC gel sandwich electrolyte. Cu is used as the working electrode, and Li is used as the reference and counter electrodes, respectively. b) Galvanostatic voltage profile of a Cu–Li battery separated with sandwich electrolyte at a current density of 200 mA g^{-1} and a voltage window of 2–4.1 V. c) The SCN-mediated charging plateaus of Cu cathode predicted by DFT simulation. d) Self-discharge test of solid-state Cu–Li batteries. e) The voltage profiles of DES gel/LATP/DES-FEC gel separated Cu–Li batteries at 100, 200, 400, 600, 800, and 1000 mA g^{-1} . f) Rate performance of the DES gel/LATP/DES-FEC gel separated Cu–Li battery. g) Long-term stability of Cu–Li batteries with DES gel/LATP/DES-FEC gel, DES gel/LATP/DES gel, and DES gel, respectively. h) Comparison of average discharge voltages and specific capacities (based on the mass of cathode material only) for representative reported rechargeable batteries employing DES-based electrolytes (hollow symbols)^[9a,b,15] and this study (solid star).

in Figure 2d) and evaporates quickly even at room temperature, owing to the low boiling point of the carbonate solvents (as seen in Supplementary Figure 5a). Such excellent thermal stability of the DES gel guarantees the safe operation of Cu–Li batteries.

XRD patterns of as-prepared $\text{Li}_{1.4}\text{Al}_{0.4}\text{Ti}_{1.6}(\text{PO}_4)_3$ (LATP) pellet show characteristic peaks of $\text{LiTi}_2(\text{PO}_4)_3$ (PDF 35-0754) (Figure 2e). The cross-sectional image of LATP pellet exhibits dense contact between particles after sintering at 960 °C (Figure 2f). The ionic conductivities of electrolytes were also examined with electrochemical impedance measurements at different temperatures. The Arrhenius plot ($\log \sigma$ versus $1000/T$) is shown in Figure 2g. The Li^+ conductivities of DES, DES gel, LATP pellet, and DES gel/LATP/DES-FEC gel and their activation energies (E_a) are summarized in Supplementary Table 1. The ionic conductivity of the DES gel/LATP/DES-FEC gel sandwich electrolyte is 0.55 mS cm^{-1} at 25 °C, which is sufficient to meet the application requirements for Cu–Li batteries.

Stable Li plating/stripping behavior is critical for the long-term cyclability and safety of Cu–Li batteries. The plating/stripping of Li in DES gel was first studied via Li|Ti half cells, and the Coulombic efficiencies were compared in Figure 3a,b and Supplementary Figure 6a. As seen in Figure 3a, the Coulombic efficiency of a Li|DES gel|Ti cell decreases with cycling and drops to 25% in the seventh cycle, accompanied by an enlarged overpotential (129 mV). It suggests the undesired consumption of newly deposited Li due to electrolyte decomposition. In sharp contrast, the Li|DES-FEC gel|Ti cell shows a high Coulombic efficiency approaching over 98% and a small overpotential (32 mV) (Figure 3b), indicating much more stable Li plating/stripping in DES-FEC based cell. This significant improvement denotes that the 10 wt% FEC additive could effectively improve the compatibility between Li metal and DES gel, therefore, promoting a much denser Li layer ($\approx 10 \mu\text{m}$) as observed on Ti current collector in the Li|DES-FEC gel|Ti cell (Figure 3c). In comparison, the Li layer in the Li|DES gel|Ti cell is much thinner, leaving a large area of bare Ti current collector exposed (Supplementary Figure 6c,d). This improvement of Li anode compatibility can also be observed in Li|Li symmetric cells (Supplementary Figure 6b). XPS data shows that the FEC-derived SEI can effectively prevent interfacial reactions between Li metal and SCN, stabilize Li plating/stripping and promote dendrite-free growth of Li (Supplementary Figure 8).^[12] Therefore, we used DES-FEC gel at the anode side to construct solid-state Cu–Li batteries.

To enable deep cycling of the Cu cathode, the gel layer must have a high capability to absorb Cu ions released during the charging process. The solubility of Cu species in the catholyte determines the practical capacity of Cu cathodes. To assess the solvating power of DES, we also prepare an FEC-based electrolyte with a LiTFSI/FEC molar ratio of 1:13, identical to that of DES liquid. Copper triflate ($\text{Cu}(\text{OTf})_2$) salt was dissolved into DES and FEC-based electrolytes, respectively, to mimic the electrochemical dissolution process of Cu. Inductively coupled plasma mass spectrometry (ICP-MS) results reveal that DES liquid can

solvate $\text{Cu}(\text{OTf})_2$ up to 0.625 mol L^{-1} , 100 times higher than that in FEC-based electrolyte (0.006 mol L^{-1}) (Figure 3d). The big solubility is ascribed to the high polarity of SCN, which has a dielectric constant of 55 at 25 °C, giving SCN a remarkable ability to separate charges compared to conventional liquid solvents ($\epsilon_{\text{CH}_3\text{CN}} = 36.6$ at 25 °C).^[13] The high Cu-ion solubility in DES liquid makes DES gel a promising reservoir of Cu ions and allows the deep cycling of Cu cathode in Cu–Li batteries, as illustrated in the following part.

The crossover of Cu ions is a persistent issue in Cu–Li batteries, which leads to a low reversible capacity and severe self-discharge. Herein we use a LATP ceramic pellet inserted in the middle to prevent the shuttle of Cu ions. To test the magnitude of Cu-ion crossover, an H-type cell was designed in which two liquids, DES-7 mol% $\text{Cu}(\text{OTf})_2$ and DES, appearing blue and colorless, were separated in left and right tanks with different membranes in the middle. The color change in the H cell is recorded via optical images at different times. As shown in Figure 3e, when the two liquids are separated with the LATP disc, there is no color change in the right tank with incremental time. In contrast, the liquid in the right tank turned light green after 96 hours and dark green after 192 hours when the LATP disc was replaced with a DES gel layer. All these results suggest that the ceramic LATP pellet can effectively block the diffusion of Cu ions compared with a DES gel.

In a brief summary, the as-prepared sandwiched electrolyte (DES gel/LATP/DES-FEC gel) exhibits the following characteristics: 1) sufficient Li^+ conductivity at room temperature (0.55 mS cm^{-1}), 2) high compatibility with Li metal anodes, 3) high Cu-ion solubility and 4) high ion selectivity to effectively block the crossover of Cu ions. All these merits pave the way for a high-performance solid-state Cu–Li battery.

The solid-state Cu–Li battery was made into a coin cell with a Cu cathode (Supplementary Figure 9) and a Li anode, separated by the solid-state sandwich electrolyte (DES gel/LATP/DES-FEC). The cathode reaction mechanism was first assessed via cyclic voltammetry (CV) test with Cu as the working electrode and Li as counter/reference electrodes. As shown in Figure 4a, two pairs of redox peaks at 2.5/2.75 V and 3.85/4.0 V (vs. Li^+/Li) are observed, demonstrating two reversible redox reactions. On the other hand, when the Cu working electrode is replaced with a stainless-steel disc, these redox peaks vanish, indicating that the reversible peaks derive from the redox reaction of the Cu cathode rather than from the stainless-steel cell casing (Figure 4a). The galvanostatic charge/discharge test of the Cu–Li battery was also performed at a constant current of 200 mA g^{-1} between 2.0 and 4.1 V. As shown in Figure 4b, the Cu electrode exhibits two charging plateaus at 2.75 V and 4.0 V (vs. Li^+/Li), consistent with the CV result. Additionally, it delivers a reversible capacity of $511 \text{ mAh g}_{\text{Cu}}^{-1}$, dramatically improved when compared with previously reported values.^[2c,6] Comparatively, a reference battery composed of an Al foil cathode, Li anode, and the same solid-state sandwich electrolyte cannot be charged/discharged (Figure 4b), implying that the capacity does not originate from

the Al current collector of the cathode. Both CV and galvanostatic charge/discharge tests reveal a two-step charging process for Cu cathodes. As we know, charging Cu involves the electrochemical dissolution of metallic Cu, accompanied by the release of Cu ions into electrolyte; metallic Cu tends to lose its 4s electrons to form monovalent (Cu^+) and divalent (Cu^{2+}) ions in solution.^[14] Therefore, it can be inferred that these two steps may correspond to Cu/Cu^+ and $\text{Cu}^+/\text{Cu}^{2+}$ conversion reactions, respectively, in which the first-step redox (Cu/Cu^+) is dissolution-controlled while the second-step redox ($\text{Cu}^+/\text{Cu}^{2+}$) is diffusion-controlled.

The SCN-mediated charging plateaus of Cu cathode in Cu–Li batteries were further predicted by density functional theory (DFT) simulation, which also confirms this two-step charging mechanism. The coordination numbers of Cu–SCN complexes were optimized first, and the charging potentials against Li^+/Li were computed from a series of energy calculations. As shown in Figure 4c, the predicted potentials for Cu/Cu^+ and $\text{Cu}^+/\text{Cu}^{2+}$ reactions in an SCN-based medium agreed well with experimental values. The as-generated Cu species were released into DES gel with the formation of stable complexes: monovalent Cu tends to form a $\text{Cu}(\text{SCN})_3$ complex with a coordination number of 3, while divalent Cu are more ready to combine 4 SCN molecules to form a complex structure with a coordination number of 4 (Supplementary Figure 10). In addition, the Cu-ion quantification in DES gels at different electrochemical states also confirms this two-step reaction mechanism. As shown in Supplementary Figure 11, Cu–Li batteries were stopped at four electrochemical states during the initial cycle of charge/discharge processes. The Cu species released in DES gel at each electrochemical state were determined by microwave digestion coupled with ICP-MS. Three samples of each electrochemical state were collected and tested in parallel to ensure reproducibility. Interestingly, no Cu species were present in a fresh gel, while 43.8 ppm Cu ions were detected in DES gel detached from the battery charged to 3.5 V (end of the first plateau). The appearance of Cu ions demonstrates the electrochemical dissolution of the Cu cathode during the charging process. The experimental value agrees well with the theoretical value obtained from the charging capacity at the cutoff voltage of 3.5 V. As revealed by DFT simulation, the capacity of this step originates from the Cu/Cu^+ conversion reaction. When further charging the battery to 4.1 V (the end of the second plateau), the amount of Cu ion in the DES gel remains the same, implying that further oxidation of Cu^+ to Cu^{2+} occurs at this step, thereby bringing no variation of Cu amount in gels at 3.5 and 4.1 V. The result of ICP-MS is consistent with the result of the DFT simulation. Similarly, a two-step discharge process was also proved with the ICP-MS test. Details can be found in Supporting Information.

The Cu-ion crossover in a Cu–Li battery was also assessed via a self-discharge test. After 3 cycles' activation at a current rate of 200 mA g^{-1} , the Cu–Li battery separated with DES gel/LATP/DES-FEC gel was charged to 4.1 V and kept at OCV for 24 hours. Then the battery was discharged to 2.0 V (Figure 3e). A Coulombic efficiency of 99.6 % can

be maintained, demonstrating this electrolyte's excellent ability to inhibit Cu-ion crossover during battery operation.

The sandwiched electrolyte (DES gel/LATP/DES-FEC gel) exhibits a high Li^+ conductivity at room temperature, enabling rapid reaction kinetics for the Cu–Li battery. The rate performance of the DES gel/LATP/DES-FEC gel separated Cu–Li battery was performed at various current densities ranging from 100 to 1000 mA g^{-1} (Figure 4e,f). As the current density increased from 100 to 1000 mA g^{-1} , the capacity of Cu decreased from 511 to 239 mAh g^{-1} , revealing high retention of 47 %. Apart from the fast Li^+ conductivity, the homogeneous Cu particles grown in the DES-based medium also promote fast battery kinetics, as revealed by SEM images and chronoamperometry (C.A.) tests in Supporting Information (Supplementary Figure 12, 13). Additional advantages of the solid-state sandwich electrolyte lie in the high Li compatibility and complete blockage of Cu-ion crossover, which enable improved cyclability of the Cu–Li battery. Figure 4g shows the long-term cycle performance of Cu–Li batteries at a current rate of 200 mA g^{-1} . Interestingly, the solid-state Cu–Li battery displays very stable cyclability over 120 cycles. In contrast, a reference Cu–Li battery separated with DES gel/LATP/DES gel shows capacity fading in later cycles, which is caused by the poor compatibility between DES gel and Li metal, as discussed above section. The Cu–Li battery separated with DES gel only delivers a small discharge capacity ($<450 \text{ mAh g}^{-1}$) in the first cycle, and the capacity fades quickly to 0 after 30 cycles, demonstrating severe Cu-ion crossover under the external electric field. Our results confirm the significantly improved capacity and cyclability of the DES gel/LATP/DES-FEC gel-separated Cu–Li battery.

The average output voltages at different current rates of Cu–Li batteries were plotted with specific capacities (Figure 4h). The energy densities were then compared with that of previously reported rechargeable batteries employing DES-based electrolytes. As shown in Figure 4h, the solid-state Cu–Li battery based on DES gel/LATP/DES-FEC gel solid electrolytes can deliver high energy densities ranging from 635 to 1485 Wh kg^{-1} when varying the currents from 1000 to 100 mA g^{-1} , which are much higher than previously reported carbonate-electrolyte-based Cu cathode batteries.^[2c,6] Therefore, it is evident that this multifunctional solid-state sandwich electrolyte effectively addresses the issues in Cu–Li batteries and significantly improves battery cyclability and energy density. It should be emphasized that this electrolyte designing strategy could also be extended to other low-cost metal cathode batteries.

Conclusion

In summary, we successfully developed a multifunctional solid-state sandwich electrolyte with a DES gel/LATP/DES-FEC gel structure for solid-state Cu–Li batteries for the first time, which exhibits 1) sufficient Li^+ conductivity at room temperature (0.55 mS cm^{-1}), 2) high compatibility with Li metal anodes, 3) high Cu-ion solubility, 4) high ion selectiv-

ity to effectively block the crossover of Cu-ion species, and 5) non-flammability. These exceptional features ensure superior cyclability with 97% capacity retention over 120 cycles and high energy density (1485 Wh kg_{Cu}⁻¹) of solid-state Cu–Li batteries. These key findings provide a deeper insight into developing solid-state Cu–Li batteries with high energy density, long-term cycling stability, and unrivaled safety. Furthermore, the electrolyte design strategy is applicable to other high-energy-density metal cathode batteries, such as nickel–Li and stainless steel–Li batteries.

Acknowledgements

This work was financially supported by the National Natural Science Foundation of China (21878189), Guangdong Basic and Applied Basic Research Foundation (2022A1515011677), Project of Educational Commission of Guangdong Province of China (2020ZDZX2011), Shenzhen Science and Technology Project Program (JCYJ20190808144413257, JCYJ20210324094204012), Shenzhen Key Projects of Technological Research (JSGG20200925145800001), Natural Sciences and Engineering Research Council of Canada (NSERC), Canada Research Chair Program (CRC), Canada Foundation for Innovation (CFI), and Ontario Research Fund (ORF). Dr. C. Wang acknowledges Banting Postdoctoral fellowships (BPF–180162).

Conflict of Interest

The authors declare no conflict of interest.

Data Availability Statement

The data that support the findings of this study are available from the corresponding author upon reasonable request.

Keywords: Cu–Li Batteries · Deep Eutectic Solvent · Metal Cathodes · Sandwich Electrolyte · Solid-State Batteries

- [1] a) M. Armand, J.-M. Tarascon, *Nature* **2008**, *451*, 652–657; b) J. W. Choi, D. Aurbach, *Nat. Rev. Mater.* **2016**, *1*, 16013; c) W. Li, J. R. Dahn, D. S. Wainwright, *Science* **1994**, *264*, 1115–1118; d) L. Suo, O. Borodin, T. Gao, M. Olguin, J. Ho, X. Fan, C. Luo, C. Wang, K. Xu, *Science* **2015**, *350*, 938–943; e) M. C. Lin, M. Gong, B. Lu, Y. Wu, D. Y. Wang, M. Guan, M. Angell, C. Chen, J. Yang, B. J. Hwang, H. Dai, *Nature* **2015**, *520*, 324–328; f) A. Ponrouch, C. Frontera, F. Barde, M. R. Palacin, *Nat. Mater.* **2016**, *15*, 169–172; g) J. Hassoun, K. S. Lee, Y. K. Sun, B. Scrosati, *J. Am. Chem. Soc.* **2011**, *133*, 3139–3143.

- [2] a) A. Jameson, A. Khazaeli, D. P. J. Barz, *J. Power Sources* **2020**, *453*, 227873; b) H. Wang, D. Y. W. Yu, *Electrochim. Acta* **2019**, *298*, 186–193; c) K. Xue, H. Wang, P.-K. Lee, S. Dong, D. Y. W. Yu, *ACS Appl. Mater. Interfaces* **2021**, *13*, 47449–47457; d) M. A. Zelinsky, J. M. Koch, K.-H. Young, *Batteries* **2017**, *4*, 1.
- [3] a) Y. Wang, H. Zhou, *Electrochem. Commun.* **2009**, *11*, 1834–1837; b) X. Dong, Y. Wang, Y. Xia, *Sci. Rep.* **2014**, *4*, 6916; c) H. Zhang, T. Yang, X. Wu, Y. Zhou, C. Yang, T. Zhu, R. Dong, *Chem. Commun.* **2015**, *51*, 7294–7297; d) Y. Huang, W. Zhang, S. Li, W. Luo, Z. Huang, C. Fang, M. Weng, J. Zheng, F. Pan, Q. Liu, Y. Huang, *Nano Energy* **2018**, *54*, 59–65.
- [4] H. Wang, K. Xue, B. Su, D. Y. W. Yu, *Electrochim. Acta* **2021**, *388*, 138595.
- [5] H. Wang, D. Y. W. Yu, *ACS Appl. Energy Mater.* **2019**, *2*, 4936–4942.
- [6] H. Wang, Y. Sun, M. Li, G. Li, K. Xue, Z. Chen, D. Y. W. Yu, *Small* **2020**, *16*, 2003438.
- [7] M. K. Tran, M.-T. F. Rodrigues, K. Kato, G. Babu, P. M. Ajayan, *Nat. Energy* **2019**, *4*, 339–345.
- [8] a) Q. Zhang, K. De Oliveira Vigier, S. Royer, F. Jerome, *Chem. Soc. Rev.* **2012**, *41*, 7108–7146; b) B.-Y. Zhao, P. Xu, F.-X. Yang, H. Wu, M.-H. Zong, W.-Y. Lou, *ACS Sustainable Chem. Eng.* **2015**, *3*, 2746–2755; c) G. García, S. Aparicio, R. Ullah, M. Atilhan, *Energy Fuels* **2015**, *29*, 2616–2644.
- [9] a) P. Jaumaux, Q. Liu, D. Zhou, X. Xu, T. Wang, Y. Wang, F. Kang, B. Li, G. Wang, *Angew. Chem. Int. Ed.* **2020**, *59*, 9134–9142; *Angew. Chem.* **2020**, *132*, 9219–9227; b) P. Jiang, L. Chen, H. Shao, S. Huang, Q. Wang, Y. Su, X. Yan, X. Liang, J. Zhang, J. Feng, Z. Liu, *ACS Energy Lett.* **2019**, *4*, 1419–1426; c) C. Wang, K. R. Adair, J. Liang, X. Li, Y. Sun, X. Li, J. Wang, Q. Sun, F. Zhao, X. Lin, R. Li, H. Huang, L. Zhang, R. Yang, S. Lu, X. Sun, *Adv. Funct. Mater.* **2019**, *29*, 1900392.
- [10] P. Whitfield, A. Abouimrane, I. Davidson, *Solid State Ionics* **2010**, *181*, 740–744.
- [11] D. Zhou, Y. Chen, B. Li, H. Fan, F. Cheng, D. Shanmukaraj, T. Rojo, M. Armand, G. Wang, *Angew. Chem. Int. Ed.* **2018**, *57*, 10168–10172; *Angew. Chem.* **2018**, *130*, 10325–10329.
- [12] Q. Zhang, K. Liu, F. Ding, W. Li, X. Liu, J. Zhang, *ACS Appl. Mater. Interfaces* **2017**, *9*, 29820–29828.
- [13] a) P. J. Alarco, Y. Abu-Lebdeh, A. Abouimrane, M. Armand, *Nat. Mater.* **2004**, *3*, 476–481; b) J. T. A. D. Berg, *J. Electrochem. Soc.* **1963**, *110*, 580–582.
- [14] a) M. Grioni, J. B. Goedkoop, R. Schoorl, F. M. de Groot, J. C. Fuggle, F. Schafers, E. E. Koch, G. Rossi, J. Esteva, R. C. Karnatak, *Phys. Rev. B: Condens. Matter Mater. Phys.* **1989**, *39*, 1541–1545; b) R. A. Bair, W. A. Goddard, *Phys. Rev. B* **1980**, *22*, 2767–2776.
- [15] a) R. Chen, F. Liu, Y. Chen, Y. Ye, Y. Huang, F. Wu, L. Li, *J. Power Sources* **2016**, *306*, 70–77; b) G. Fu, S. Buddhironon, N. Kim, A. Seko, K. Adachi, Y. Tsukahara, T. Kyu, *Polymer* **2018**, *159*, 64–74; c) B. Joos, T. Vranken, W. Marchal, M. Safari, M. K. Van Bael, A. T. Hardy, *Chem. Mater.* **2018**, *30*, 655–662; d) J. Zhao, J. Zhang, W. Yang, B. Chen, Z. Zhao, H. Qiu, S. Dong, X. Zhou, G. Cui, L. Chen, *Nano Energy* **2019**, *57*, 625–634; e) W. Kao-ian, R. Pornprasertsuk, P. Thamyongkit, T. Maiyalagan, S. Kheawhom, *J. Electrochem. Soc.* **2019**, *166*, A1063–A1069.

Manuscript received: September 26, 2022

Accepted manuscript online: November 14, 2022

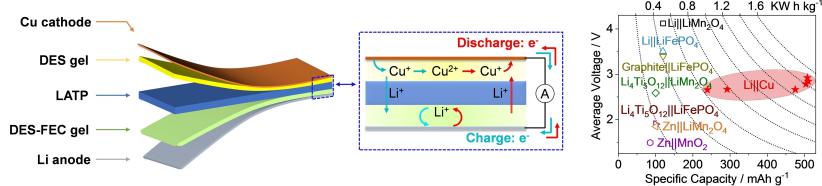
Version of record online: ■■■■■

Research Articles

Solid-state Batteries

H. Wang, C. Wang, M. Zheng, J. Liang,
M. Yang, X. Feng, X. Ren, D. Y. W. Yu, Y. Li,*
X. Sun* **e202214117**

A Shuttle-Free Solid-State Cu–Li Battery
Based on a Sandwich-Structured Electrolyte



Low-cost Cu–Li batteries leveraging Cu cathode dissolution/deposition have been hindered by electrolyte related issues, including Cu crossover, low conductivity, etc. Here the authors design a sandwich solid-state electrolyte by sand-

wiching a $\text{Li}_{1.4}\text{Al}_{0.4}\text{Ti}_{1.6}(\text{PO}_4)_3$ pellet with two deep-eutectic-solvent gels to address these issues. The as-prepared solid-state Cu–Li battery exhibits significantly improved cyclability and practical energy density.